Article

Discovery Medicine 2026; 38(211): 2620–2633
https://doi.org/10.24976/Discov.Med.202638211.206

Comparison of Early- and Late-Stage *EGFR*-Mutated Lung Adenocarcinomas Using Spatial Transcriptomics

Lingyi Yang[1,†], Cheng Chen[1,†], Xurui Shen[1], Songbai Liu[2], Zaixiang Tang[3,*], Hualong Qin[4,*]

[1]Department of Pulmonary and Critical Care Medicine, The First Affiliated Hospital of Soochow University, 215006 Suzhou, Jiangsu, China
[2]Jiangsu Province Engineering Research Center of Molecular Target Therapy and Companion Diagnostics in Oncology, Suzhou Vocational Health College, 215009 Suzhou, Jiangsu, China
[3]Department of Biostatistics, School of Public Health, Suzhou Medical College of Soochow University, 215123 Suzhou, Jiangsu, China
[4]Department of Thoracic Surgery, The First Affiliated Hospital of Soochow University, 215006 Suzhou, Jiangsu, China
*Correspondence: tangzx@suda.edu.cn (Zaixiang Tang); hlqin09@163.com (Hualong Qin)
[†]These authors contributed equally.
Submitted: 31 March 2026 Revised: 27 May 2026 Accepted: 17 June 2026 Published: 24 August 2026

Background: The epidermal growth factor receptor (*EGFR*)-mutated lung adenocarcinoma (LUAD) exhibits significant stage-dependent molecular and spatial heterogeneity, which remains incompletely characterized. Elucidating stage-associated differences in gene expression, signaling pathways, and immune landscapes is critical for developing stage-stratified precision therapy for *EGFR*-mutated LUAD.

Methods: This study integrated bulk transcriptome profiling and digital spatial profiling (DSP) to investigate pathological stage-associated differences. DSP was applied to 23 *EGFR*-mutated LUAD patients (18 early-stage and 5 late-stage) to elucidate spatial heterogeneity across three tissue compartments: tumor cells, immune cells, and macrophages. Public bulk RNA sequencing data from 38 patients with *EGFR*-mutated LUAD, including 29 early-stage (I+II) and 9 late-stage (III+IV) cases, were analyzed.

Results: Bulk RNA sequencing identified 580 differentially expressed genes between early- and late-stage *EGFR*-mutated LUAD. Late-stage tumors exhibited enhanced proliferation, marked by elevated E2F, G2M checkpoint, and MYC activities, alongside activated cell cycle, DNA replication, and DNA repair pathways. Notable metabolic reprogramming was also observed, including upregulated serine and purine metabolism. Spatial transcriptomic analysis confirmed increased proliferative, oncogenic, metastatic, and glycolytic signatures in late-stage tumor cells, consistent with findings from bulk RNA sequencing. Pathway enrichment analysis across distinct compartments revealed six stage and compartment specific modules, with modules related to cell cycle, DNA repair, invasion, and metabolism significantly upregulated in the late-stage tumor cell segment. Moreover, late-stage tumors displayed an increase in exhausted $CD8^+$ T cells and elevated expression of immune checkpoints (PD-L2, PVR in tumor cells; B7-H3, LAG3 in immune cells), contributing to an immunosuppressive microenvironment.

Conclusions: These findings delineate stage-specific transcriptional, metabolic, and spatial immune reprogramming during the progression of *EGFR*-mutated LUAD. These results may provide new insights into the molecular mechanisms underlying tumor progression and identify potential targets for stage-stratified precision therapy in *EGFR*-mutated LUAD.

Keywords: *EGFR* mutation; LUAD; pathological stage; digital spatial profiling; spatial transcriptome; tumor microenvironment

Introduction

Lung adenocarcinoma (LUAD) represents the predominant histological subtype of lung cancer, responsible for roughly 40% of global lung cancer incidence [1,2]. Among the LUAD patient population, mutations in the epidermal growth factor receptor (*EGFR*) gene stand among the most prevalent oncogenic drivers, with particularly high frequencies observed in Asian individuals, never-smokers, and female patients [1,3,4,5]. The clinical implementation of EGFR tyrosine kinase inhibitors (EGFR-TKIs) has dramatically prolonged progression-free survival (PFS) and overall survival (OS) in patients harboring *EGFR*-mutated LUAD, thereby reshaping the therapeutic landscape of this malignancy [6,7,8]. Despite these advances, the clinical outcome of patients with late-stage *EGFR*-mutated LUAD remains unsatisfactory, as nearly all patients eventually develop acquired resistance to TKIs and experience disease progression [9,10,11]. By comparison, patients with early-stage *EGFR*-mutated LUAD generally exhibit more favorable outcomes following surgical resection; nevertheless, a substantial subset still suffers from tumor recurrence and distant metastasis [12,13,14]. The biological mechanisms underlying the starkly divergent clinical behaviors between early and late-stage *EGFR*-mutated LUAD remain incompletely understood.

The tumor microenvironment (TME) constitutes a complex multicellular ecosystem comprising immune cells,

stromal components, extracellular matrix, and a diverse array of soluble mediators [15,16]. It exerts a pivotal regulatory function in tumor initiation, malignant progression, metastatic dissemination, and therapeutic responsiveness [16,17,18]. In the context of *EGFR*-mutated LUAD, accumulating evidence has linked the TME to TKI resistance and clinical prognosis [19,20,21]. However, most previous investigations into the immune microenvironment of *EGFR*-mutated LUAD have relied on bulk tissue profiling, which integrates signals across heterogeneous cell populations and spatial compartments, thus masking the spatial heterogeneity inherent to the tumor immune microenvironment.

Digital Spatial Profiling (DSP) represents a cutting-edge spatial multi-omics platform that allows for high-plex, spatially resolved quantification of proteins and RNA targets in formalin-fixed, paraffin-embedded (FFPE) specimens [22]. In contrast to conventional approaches such as immunohistochemistry (IHC) and immunofluorescence (IF), which are restricted to a limited number of biomarkers, DSP permits simultaneous whole-transcriptome or high-plex protein profiling, enabling a holistic dissection of cellular composition and functional states within the TME. Additionally, DSP facilitates precise microdissection of predefined regions of interest (ROIs), including tumor cores, invasive fronts, stromal zones, and immune cell aggregates, enabling direct comparative analyses of molecular signatures across distinct spatial domains. These unique advantages establish DSP as a powerful tool for elucidating spatial immune heterogeneity in solid tumors.

To date, systematic investigations comparing the spatial immune architecture of the TME between early and late *EGFR*-mutated LUAD remain scarce. Elucidating the dynamic immune alterations throughout disease progression may uncover critical immune regulators driving malignant progression and reveal novel therapeutic vulnerabilities in late-stage disease. Accordingly, the present study employed DSP technology to conduct an in-depth, spatially resolved analysis of protein expression profiles within the TME of early-stage and late-stage *EGFR*-mutated LUAD specimens. The objectives were threefold: (1) to delineate disparities in immune cell composition and spatial distribution between early and late *EGFR*-mutated LUAD; (2) to identify key immune-associated molecules exhibiting differential spatial expression across disease stages; and (3) to evaluate potential associations between these spatial immune features and clinical outcomes. These findings are expected to provide new mechanistic insights into the progression of *EGFR*-mutated LUAD and facilitate the rational design of improved therapeutic strategies for patients with late-stage disease.

Methods

Study Population and Sample Collection

A total of 23 FFPE tissue specimens were included in this study. All samples were obtained from patients diagnosed with LUAD)carrying *EGFR* mutations, consisting of either the L858R point mutation or exon 19 deletion (19Del). These specimens were prospectively collected at the First Affiliated Hospital of Soochow University from August 2025 to December 2025. Patients with a history of previous anti-tumor therapies were excluded from the study. All patients enrolled in this study provided written informed consent prior to participation. Ethical approval was granted by the Ethics Committee of the First Affiliated Hospital of Soochow University (approval number: [2025]480).

Sample Processing and ROI Annotation for GeoMx DSP Analysis

FFPE blocks were generated from the 23 *EGFR*-mutated LUAD specimens included in the DSP analysis, and a tissue microarray (TMA) was subsequently constructed. For each patient, 2–3 tumor tissue cores with a diameter of 3 mm were selected to guarantee sufficient representation of tumor histomorphology. Subsequently, 5-µm-thick sections were prepared from the FFPE TMA and processed following a standardized experimental protocol [22]. Slides were then loaded onto the GeoMx Digital Spatial Profiler for region of interest (ROI) selection, guided by immunofluorescence staining.

For automated segmentation, customized UV illumination masks were applied to define three distinct morphologically relevant areas of illumination (AOIs): $PanCK^+$ tumor cells, $CD45^+$ immune cells, and $CD68^+$ macrophages. These AOIs were targeted for photocleavable tag release. The cleaved oligonucleotide barcodes from each AOI were then collected, extracted, and quantitatively analyzed via next-generation sequencing.

DSP Data Processing and Bioinformatic Analysis

Sequenced FASTQ files were processed using the GeoMx NGS Pipeline (version 2.2.0.2, NanoString Technologies, Inc., Seattle, WA, USA) to generate digital count conversion (DCC) files. Subsequent data quality control (QC) was performed to assess key technical metrics, including technical signal intensity, background noise levels, probe efficiency, and normalization parameters, in strict accordance with previously established guidelines [22]. Prior to initiating downstream analytical workflows, high-quality datasets were subjected to Quantile 3 (Q3) normalization [23] to ensure data consistency and reliability.

Initially, the filterByExpr function (with default parameters) was employed to exclude lowly expressed genes that could introduce noise into the analysis. Subsequently, the estimateGLMCommonDisp, estimateGLMTrended-

Disp, and estimateGLMTagwiseDisp functions (all run with default settings) were utilized to calculate common, trended, and tagwise dispersions, respectively. A negative binomial model was then fitted for each individual gene using the glmFit function. Finally, the glmLRT function, a tool that performs a likelihood ratio test to compare the goodness of fit between the experimental model and the null model, was used to determine the statistical significance of differential gene expression.

Differentially expressed genes (DEGs) were identified using stringent thresholds: a false discovery rate (FDR) of <0.05 and an absolute log2 fold change (|log2 FC|) of > 1. Gene Ontology (GO) enrichment analysis was conducted with the R package clusterProfiler, where statistical significance was defined as an FDR-corrected *p*-value of <0.05. Signature scores were calculated using the formula: $\sqrt[n]{(X_1+1)\ldots(X_i+1)\ldots(X_n+1)}$, where X_i represents the normalized expression value of genes associated with the target cell population, and n denotes the total number of genes in the signature [24]. To evaluate intergroup differences in various signatures, single-sample gene set enrichment analysis (ssGSEA) [25] was applied to the normalized gene expression matrix. The DSP data generated in this study have been deposited in the GSA-Human repository under the accession number HRA011725 (https://ngdc.cncb.ac.cn/gsa-human/browse/HRA011725).

Acquisition and Bioinformatic Analysis of Public Transcriptomic Datasets

Publicly available transcriptomic profiles and corresponding clinical metadata for 38 patients with *EGFR*-mutated LUAD, including those harboring L858R or 19Del, were retrieved from The Cancer Genome Atlas (TCGA) database. The detailed clinicopathological features of these 38 LUAD patients are summarized in **Supplementary Table 1**.

Raw read count data were processed and analyzed using the edgeR package (v3.34.0) to identify DEGs. Genes with a *p*-value < 0.05 and an absolute log2 fold change (|log2 FC|) >1 were defined as significantly differentially expressed. Volcano plots and heatmaps were generated using the ggpubr and ComplexHeatmap packages in R, respectively. Kyoto Encyclopedia of Genes and Genomes (KEGG) pathway enrichment analysis was performed using the KOBAS-i online tool [26,27,28], with statistical significance defined as a Benjamini-Hochberg adjusted *p*-value < 0.05. Intergroup differences in multiple biological signatures, were evaluated using ssGSEA [25] based on the normalized gene expression matrix.

Functional and Immune Profiling by Single-Sample Gene Set Enrichment Analysis

To comprehensively evaluate metabolic status and hallmark signaling pathway activity, ssGSEA (implemented in the GSVA R package) [25] was applied to both the DSP dataset and the public transcriptomic data. Immune cell composition across groups was calculated by ImmuneCellAI [29].

The log2-transformed normalized gene expression matrix was used for ssGSEA analysis with gene sets obtained from the WikiPathways database [30]. Non-redundant biological pathways appropriate for ssGSEA were extracted from WikiPathways [31], with analytical procedures adapted from previously published studies [31,32]. Specifically, all curated pathways were classified into seven functional clusters following a previously published study [31]. One cluster covered biological processes associated with cell proliferation and DNA damage repair, two clusters were linked to mitochondrial function and lipid metabolism, and one cluster was enriched in signatures related to tumor progression. Another cluster mainly contained immune-related signaling cascades that are frequently dysregulated during tumorigenesis. The remaining two clusters comprised transforming growth factor-β (TGF-β) receptor signaling, focal adhesion, matrix metalloproteinase activity, and neovascularization pathways, all of which promote malignant progression of tumors.

Hallmark signaling pathway scores were calculated using the hallmark gene sets from the Molecular Signatures Database (MSigDB). Finally, enrichment scores for immune cell populations within the tumor microenvironment were estimated using ssGSEA with a previously established gene signature [33].

Statistical Analysis

Between-group comparisons were performed using the Wilcoxon rank-sum test. Heatmaps were visualized using the R package "ComplexHeatmap" (v2.8.0) [34]. The "complete" agglomeration method was adopted to generate the heatmap. Statistical significance for screening gene signatures, WikiPathways pathways, immune cell subsets and immune checkpoint molecules was determined using adjusted *p* values < 0.05 after Benjamini–Hochberg multiple testing correction.

Results

Dissection of Pathological Stage-Associated Differences in Gene Expression and Signatures in EGFR-Mutated LUAD Using Bulk Transcriptome Profiling

To dissect the molecular distinctions between early-stage and late-stage tumors, publicly available RNA-sequencing datasets were analyzed (clinical information is provided in **Supplementary Table 1**). Transcriptomic profiles from lung samples of 38 patients with *EGFR*-mutated LUAD (harboring L858R or 19Del) were examined, comprising 29 early-stage and 9 late-stage cases. This analysis identified a total of 580 DEGs between the two stage groups, with 268 genes upregulated and 312 genes

downregulated in late-stage tumors (Fig. 1A; **Supplementary Table 2**). Functional enrichment analysis revealed that genes upregulated in late-stage (III+IV) tumors were significantly enriched in biological processes associated with mesodermal cell fate determination and commitment, mesoderm formation and morphogenesis, as well as regulation of the RIG-I-like receptor signaling pathway and viral transport (all adjusted p-value < 0.05; Fig. 1B, left panel). In contrast, genes upregulated in early-stage (I+II) tumors were predominantly enriched for cilium/flagellum structure and motility, along with terms related to immunoglobulin production and extracellular transport (all adjusted p-value < 0.05; Fig. 1B, right panel). These findings highlight two functionally distinct programs: one focused on antiviral defense and mesodermal lineage specification (III+IV) and another centered on ciliary dynamics and associated immune/transport functions (I+II).

Characterization of cancer-related cellular functions, signaling pathways, and metabolic signatures in *EGFR*-mutated LUAD, particularly in a stage-specific context, remains underexplored. Compared to early-stage tumors (stages I+II), late-stage tumors (stages III+IV) exhibited significantly elevated activity across multiple proliferation-related signatures, including E2F targets, G2M checkpoint, MYC targets V1, and MYC targets V2 (all $p < 0.05$; Fig. 1C,D, **Supplementary Fig. 1A,B**). With respect to signaling pathways, late-stage tumors demonstrated significantly increased activity of MTORC1 signaling and unfolded protein response, while IL2-STAT5 signaling was significantly downregulated (all $p < 0.05$; Fig. 1C,D, **Supplementary Fig. 1A,B**). Additionally, the glycolytic metabolic pathway exhibited significant upregulation in late-stage tumors ($p < 0.05$; Fig. 1C,D, **Supplementary Fig. 1A,B**). These findings indicate that the progression of *EGFR*-mutated LUAD from early to late stages is accompanied by distinct molecular alterations, including elevated proliferative potential, aberrant signaling activity, inhibited immune pathways, and a metabolic shift toward glycolysis. These molecular changes are closely associated with malignant progression and potential therapeutic resistance.

Stage-Specific Pathways in EGFR-Mutated LUAD Revealed by Bulk Transcriptome Profiling

To comprehensively evaluate pathway differences across clinical stages, pathway enrichment analysis was conducted using a curated dataset from the WikiPathways database [29]. This analysis identified seven distinct pathway clusters (C1-C7) that distinguished early-stage from late-stage tumors (Fig. 2A). pathways in the C2 cluster, associated with immune-related signatures, were predominantly active in the early-stage group (Fig. 2A,B, **Supplementary Fig. 2A,B**). In contrast to late-stage tumors, early-stage tumors exhibited significantly higher activity scores for the B cell receptor signaling pathway, components involved in local acute inflammatory response, and complement activation (all $p < 0.05$; Fig. 2B and **Supplementary Fig. 2B**). These findings indicate a more robust immune surveillance and acute inflammatory response in early-stage disease, reflecting the host's attempt to restrict tumor initiation and progression via humoral immunity, innate immune activation, and complement-mediated tumor clearance. Conversely, C5-clustered pathways showed elevated activity scores in the late-stage group, including those related to cell cycle progression, DNA replication, G1 to S cell cycle control, and multiple DNA repair pathways (all $p < 0.05$; Fig. 2B and **Supplementary Fig. 2B**). This indicates a profound rewiring of proliferative and genome maintenance networks to support uncontrolled growth and genomic instability in late-stage disease. Additionally, pathways related to metabolic and nucleotide biosynthesis were significantly upregulated in late-stage tumors (all $p < 0.05$; Fig. 2B and **Supplementary Fig. 2B**). Specifically, serine metabolism and purine metabolism exhibited markedly higher estimated scores in late-stage tumors compared with early-stage tumors (both $p < 0.05$; Fig. 2B and **Supplementary Fig. 2B**), highlighting an increased reliance on de novo serine synthesis and purine biosynthesis to support rapid proliferation and biomass accumulation in the later disease stages. Concomitantly, metabolic reprogramming was also significantly elevated in the III+IV group ($p < 0.05$; Fig. 2B and **Supplementary Fig. 2B**), consistent with the Warburg effect and metabolic adaptation to the tumor microenvironment (TME).

Stage-Stratified Spatial Transcriptomic Characterization of Intratumoral Regions in EGFR-Mutated LUAD via DSP

Bulk RNA-sequencing approaches inherently mask intratumoral complexity and fail to resolve the spatial architecture of the tissue microenvironment. To address this critical limitation, the spatial heterogeneity of tumor cells and the TME in *EGFR*-mutated LUAD was dissected, with a specific focus on their associations with pathological stages, utilizing a previously established spatially resolved multiplexed digital spatial profiling (DSP) dataset [35]. A total of 23 patients with *EGFR*-mutated LUAD were included for DSP analyses, comprising 18 early-stage cases (15 stage I and 3 stage II) and 5 late-stage cases (4 stage III and 1 stage IV) (**Supplementary Table 3**). Three molecularly distinct tissue compartments were identified and analyzed based on fluorescent co-localization patterns, including PanCK$^+$ tumor cells (PanCK$^+$/CD45$^-$/SYTO13$^+$), CD45$^+$ immune cells (PanCK$^-$/CD45$^+$/CD68$^-$/SYTO13$^+$), and CD68$^+$ macrophages (PanCK$^-$/CD68$^+$/SYTO13$^+$) (Fig. 3A). Details of ROIs and AOIs are summarized in **Supplementary Fig. 3A**.

First, DEGs and enriched biological processes in spatially distinct compartments were identified between early-stage and late-stage patients. In the PanCK$^+$ tumor cell compartment, 351 DEGs were detected between late-stage

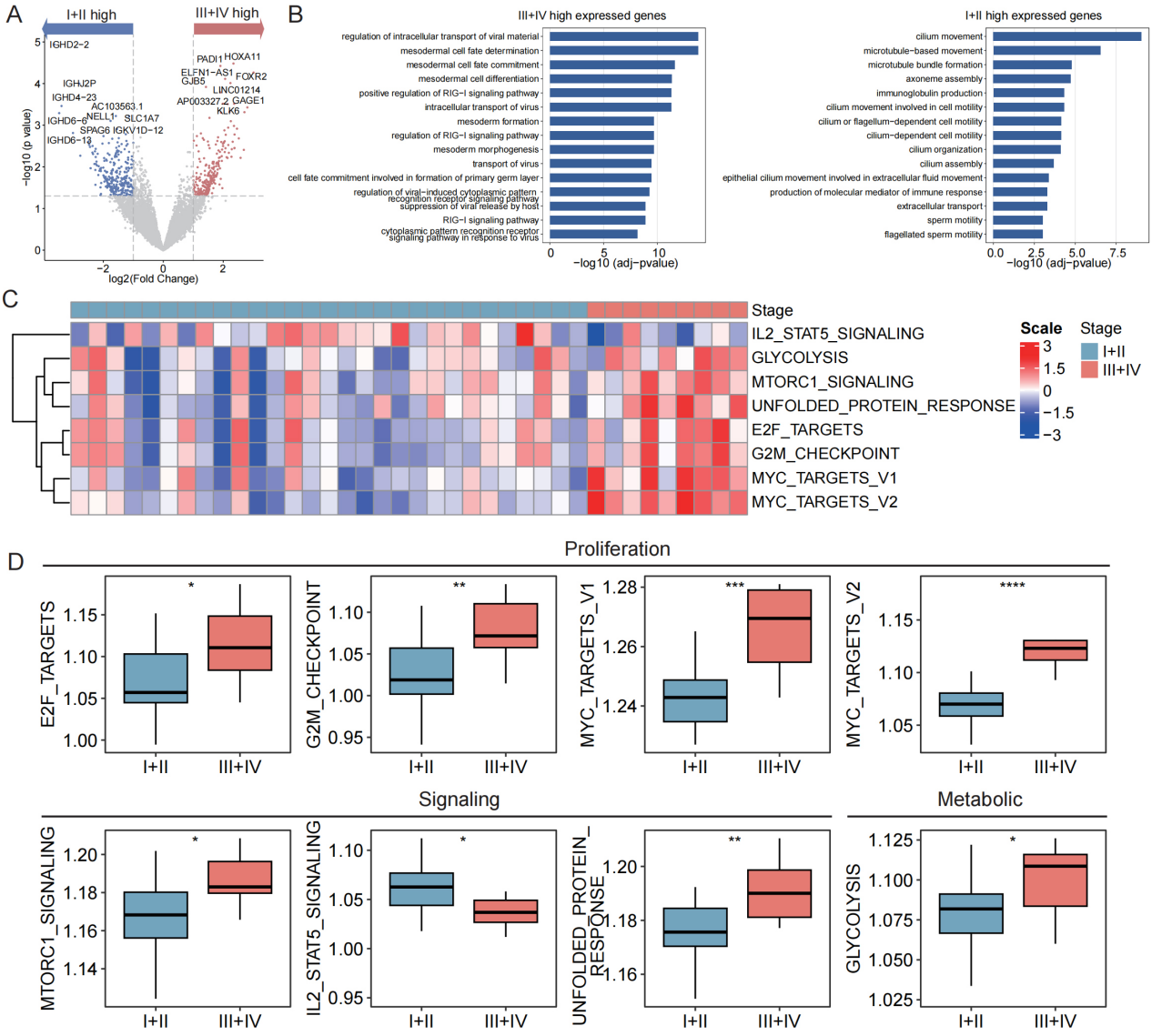

Fig. 1. Stage-related gene expression profiles and functional enrichment in *EGFR*-mutated LUAD. (A) Volcano plot of differentially expressed genes between early and late stages. Red and blue points represent genes that are significantly upregulated in late-stage and early-stage tumors, respectively. Genes with no significant changes are shown in gray. (B) Enriched Gene Ontology (GO) biological processes for genes upregulated in late-stage (left) and early-stage (right) tumors, respectively. (C) Heatmap showing enrichment levels of signatures associated with proliferation, signaling, and metabolic activity across early (n = 29) and late (n = 9) stages. (D) Boxplots comparing the enrichment scores of proliferation, signaling, and metabolic signatures between early (n = 29) and late (n = 9) stages. EGFR, epidermal growth factor receptor; LUAD, lung adenocarcinomas; GO, gene ontology. *$p < 0.05$, **$p < 0.01$, ***$p < 0.001$, ****$p < 0.0001$.

and early-stage cohorts, comprising 230 upregulated and 121 downregulated genes in late-stage tumors (Fig. 3B, left panel; **Supplementary Table 4A**). GO enrichment analysis within the PanCK$^+$ tumor cell segment revealed two distinct epithelial programs. Genes upregulated in the late stage were enriched for processes related to immune tolerance induction, cell adhesion, and nucleosome assembly (**Supplementary Fig. 3B**; left panel). In contrast, genes upregulated in the early stage were predominantly associated with antigen processing and presentation via MHC class II, T cell activation, and extracellular matrix organization (**Supplementary Fig. 3B**; right panel). These findings highlight functionally distinct states: one oriented toward immune tolerance (late stage) and another focused on antigen presentation and immunostimulation (early stage). Within the CD45$^+$ immune cell segment, 213 DEGs were identified between late-stage and early-stage patients, with 61 genes highly expressed in late-stage patients and 152

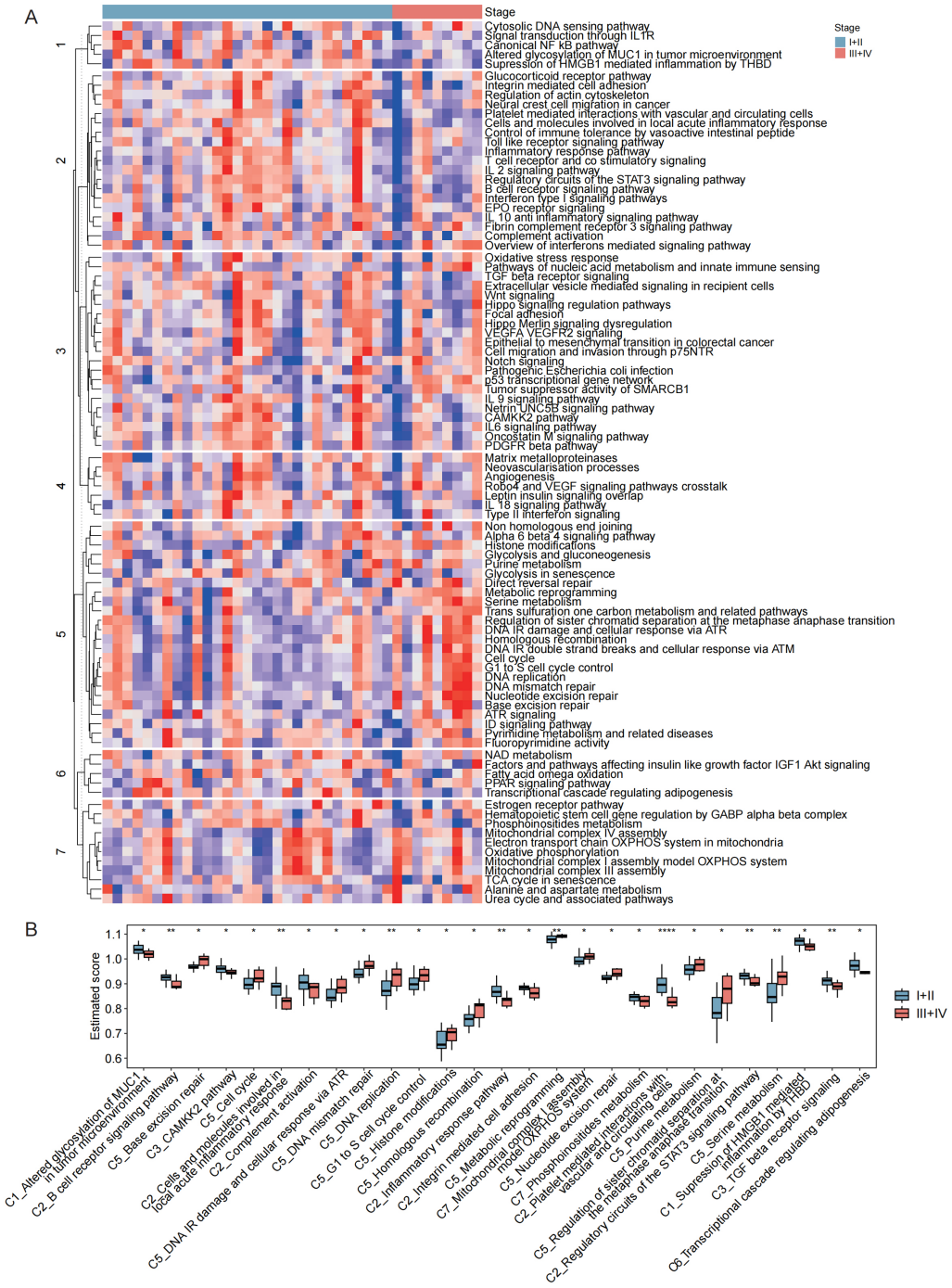

Fig. 2. Key biological pathways associated with tumor stage. (A) Heatmap of unsupervised clustering based on ssGSEA scores derived from gene sets in the WikiPathways database. Major clusters of dysregulated pathways are indicated by white horizontal lines. I+II stage (n = 29); III+IV stage (n = 9). (B) Boxplots showing pathways that are significantly associated with tumor stage. ssGSEA, single sample gene set enrichment. I+II stage (n = 29); III+IV stage (n = 9). *$p < 0.05$, **$p < 0.01$, ****$p < 0.0001$.

genes in early-stage patients (Fig. 3B, middle panel; **Supplementary Table 4B**). In the CD68$^+$ macrophage compartment, 465 genes exhibited significant expression differences with 150 upregulated and 315 downregulated in late-stage compared to early-stage tumors (Fig. 3B, right panel; **Supplementary Table 4C**). GO biological process enrichment analysis revealed that the top enriched terms in the CD45$^+$ immune cell and CD68$^+$ macrophage segment of late-stage patients were both linked to extracellular matrix organization (**Supplementary Fig. 3C,D**), a biological process known to influence various hallmarks of cancer [36,37,38].

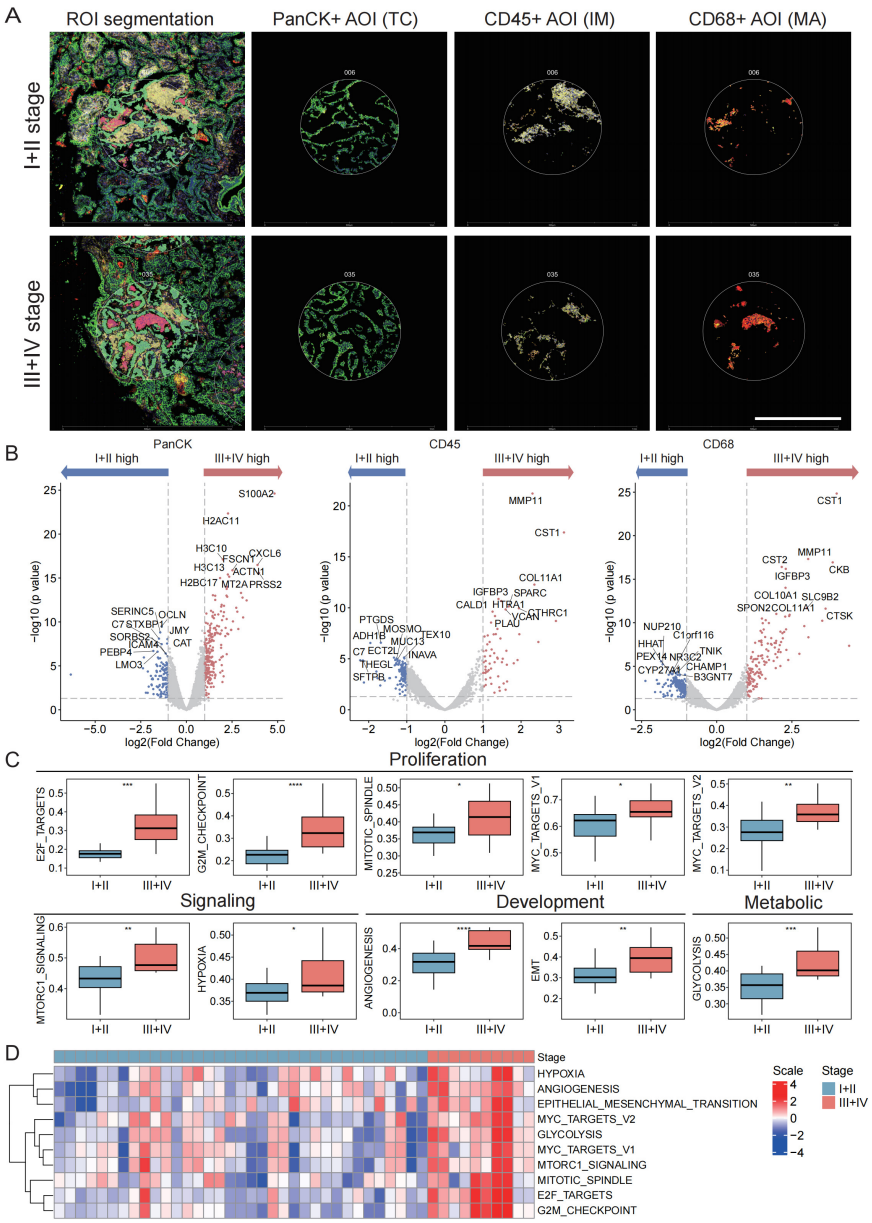

Fig. 3. Spatial transcriptomic profiling identifies stage-associated gene expression and functional signatures across distinct tissue compartments in *EGFR*-mutated LUAD. (A) Representative regions of interest (ROIs) and areas of illumination (AOIs). AOIs were defined for DSP analysis based on immunofluorescence staining for PanCK (green), CD45 (yellow), CD68 (red), and SYTO13 (blue). Scale bar = 500 µm. (B) Volcano plots showing differentially expressed genes between early- and late-stage AOIs across distinct compartments: PanCK$^+$ tumor cell compartment (left), CD45$^+$ immune cell compartment (middle), and CD68$^+$ macrophage compartment (right). Red and blue points represent genes significantly upregulated in late-stage and early-stage groups, respectively. Genes with no significant differences are shown in gray. (C) Boxplots comparing enrichment scores of proliferation, signaling, developmental, and metabolic signatures between early-stage (35 AOIs) and late-stage (10 AOIs) groups within the PanCK$^+$ tumor cell compartment. (D) Heatmap showing expression levels of signatures associated with proliferation, signaling, developmental processes, and metabolic activity between early-stage (35 AOIs) and late-stage (10 AOIs) groups. EGFR, epidermal growth factor receptor; LUAD, lung adenocarcinomas; DSP, digital spatial profiling; ROIs, regions of interest; AOIs, areas of illumination; PanCK, pan-cytokeratin. *$p < 0.05$, **$p < 0.01$, ***$p < 0.001$, ****$p < 0.0001$.

The spatial characterization of cancer-associated cellular functions, signaling pathways, and metabolic signatures in *EGFR*-mutated LUAD remains largely unexplored, particularly in the context of clinical staging. In the PanCK$^+$

tumor cell compartment, the late-stage subgroup exhibited significantly elevated enrichment scores across multiple oncogenic pathways compared with the early-stage subgroup (Fig. 3C,D, **Supplementary Fig. 4A,B**). Specifically, proliferation-related signatures, including E2F targets, G2M checkpoint, mitotic spindle, and MYC targets V1/V2, were markedly activated in the late-stage subgroup (all $p < 0.05$; Fig. 3C,D, **Supplementary Fig. 4A,B**). Concurrently, oncogenic signaling pathways such as MTORC1 signaling and hypoxia were significantly upregulated in late-stage tumors (both $p < 0.05$; Fig. 3C,D, **Supplementary Fig. 4A,B**). Furthermore, signatures associated with tumor development and metastasis, namely angiogenesis and epithelial-mesenchymal transition (EMT), displayed strikingly higher activity in the late subgroup (both $p < 0.05$; Fig. 3C,D, **Supplementary Fig. 4A,B**). Metabolically, the glycolysis pathway, a well-recognized hallmark of cancer, was also significantly enhanced in late-stage *EGFR*-mutated LUAD ($p < 0.05$; Fig. 3C,D, **Supplementary Fig. 4A,B**). These spatially resolved findings were consistent with the transcriptional profiles obtained from public bulk RNA sequencing datasets (Fig. 1C,D, and **Supplementary Fig. 1**). These results indicate that the late-stage group is characterized by a more aggressive phenotypic state, defined by enahnced proliferative capacity, metabolic reprogramming, and increased metastatic potential relative to the early-stage group.

Distinct Biological Processes Associated With Pathological Stages in Each Compartment

To characterize the spatial and stage-dependent regulation of oncogenic pathways in *EGFR*-mutated LUAD, pathway enrichment analysis was performed across three distinct tissue segments (PanCK$^+$ tumor cells, CD45$^+$ immune cells, and CD68$^+$ macrophages), stratified by clinical stage (I+II vs. III+IV). Unsupervised hierarchical clustering of enrichment scores identified six functionally distinct modules, each exhibiting unique spatial distribution and stage-specific activation patterns (Fig. 4A). Modules 1, 2, and 3, which encompass metabolic, immunoregulatory, and inflammatory programs, were primarily active in the CD45$^+$ immune cell and/or CD68$^+$ macrophage compartments. In contrast, Modules 4 and 5, including key drivers of tumor progression (e.g., VEGFA/VEGFR2 signaling, TGFβ receptor signaling, EMT, focal adhesion) and genomic stability (e.g., cell cycle, DNA replication, DNA repair), displayed a striking specificity for PanCK$^+$ tumor cell, with maximal activation observed in late-stage samples. Module 6, represented by alanine and aspartate metabolism, showed negligible variation across all segments and stages.

A focused analysis of the PanCK$^+$ tumor cell compartment confirmed that stage III+IV tumors exhibited significant upregulation of pathways governing cell cycle progression (e.g., cell cycle, G1 to S cell cycle control, DNA replication), DNA damage repair (e.g., base excision repair, DNA mismatch repair, ATR-mediated DNA damage response), and cell migration/invasion (e.g., p75NTR-mediated migration, focal adhesion, Integrin signaling), conjunction with enhanced metabolic activity (e.g., NAD metabolism, metabolic reprogramming) (Fig. 4B). Most of these spatially resolved findings were consistent with the transcriptional profiles derived from bulk RNA-seq analyses (Fig. 2B and **Supplementary Fig. 2B**). These data illustrate a highly compartmentalized and stage-dependent activation of oncogenic programs, wherein late-stage *EGFR*-mutated LUAD is defined by the coordinated upregulation of proliferative, invasive, and metabolic pathways within the tumor epithelial compartment.

Immune-Related Differences Associated With Pathological Stages

To characterize the immune landscape and checkpoint regulation across pathological stages in *EGFR*-mutated LUAD, the immune cell composition and expression of immunomodulatory molecules were analyzed in a spatially resolved manner. Unsupervised clustering of immune cell subset abundances revealed distinct immune profiles between early and late stages within the CD45$^+$ immune cell compartment (Fig. 5A). Notably, late-stage tumors exhibited a significant increase in exhausted CD8$^+$ T cells (Fig. 5B), an established hallmark of impaired anti-tumor immunity. Conversely, early-stage samples displayed higher proportions of naïve CD8$^+$ T cells and monocytes in the CD45$^+$ immune cell compartment (Fig. 5B), which are critical for initiating and sustaining effective anti-tumor immune responses.

Analysis of immunoregulatory gene expression across tissue segments identified a stage-dependent upregulation of multiple immune checkpoints (Fig. 5C). Key molecules, including *PDCD1LG2* (PD-L2) and *PVR*, were significantly elevated in the PanCK$^+$ tumor cell compartment of late-stage samples. In contrast, CD47 was upregulated in the PanCK$^+$ tumor cell compartment of early-stage samples, while CD276 (B7-H3) and LAG3 expression levels were increased in the CD45$^+$ immune cell compartment of late-stage samples (Fig. 5D and **Supplementary Fig. 5A–C**). Notably, these molecules are known to mediate critical inhibitory signals: CD47 and PVR function as “don’t eat me” signals that evade phagocytosis, while PD-L2, B7-H3, and LAG3 directly suppress T cell effector function. These findings highlight a compartmentalized and stage-specific immune suppression program, wherein late-stage *EGFR*-mutated LUAD is characterized by both T cell exhaustion and the upregulation of multiple inhibitory checkpoint signals, collectively creating a robust immunosuppressive microenvironment that facilitates immune evasion and disease progression.

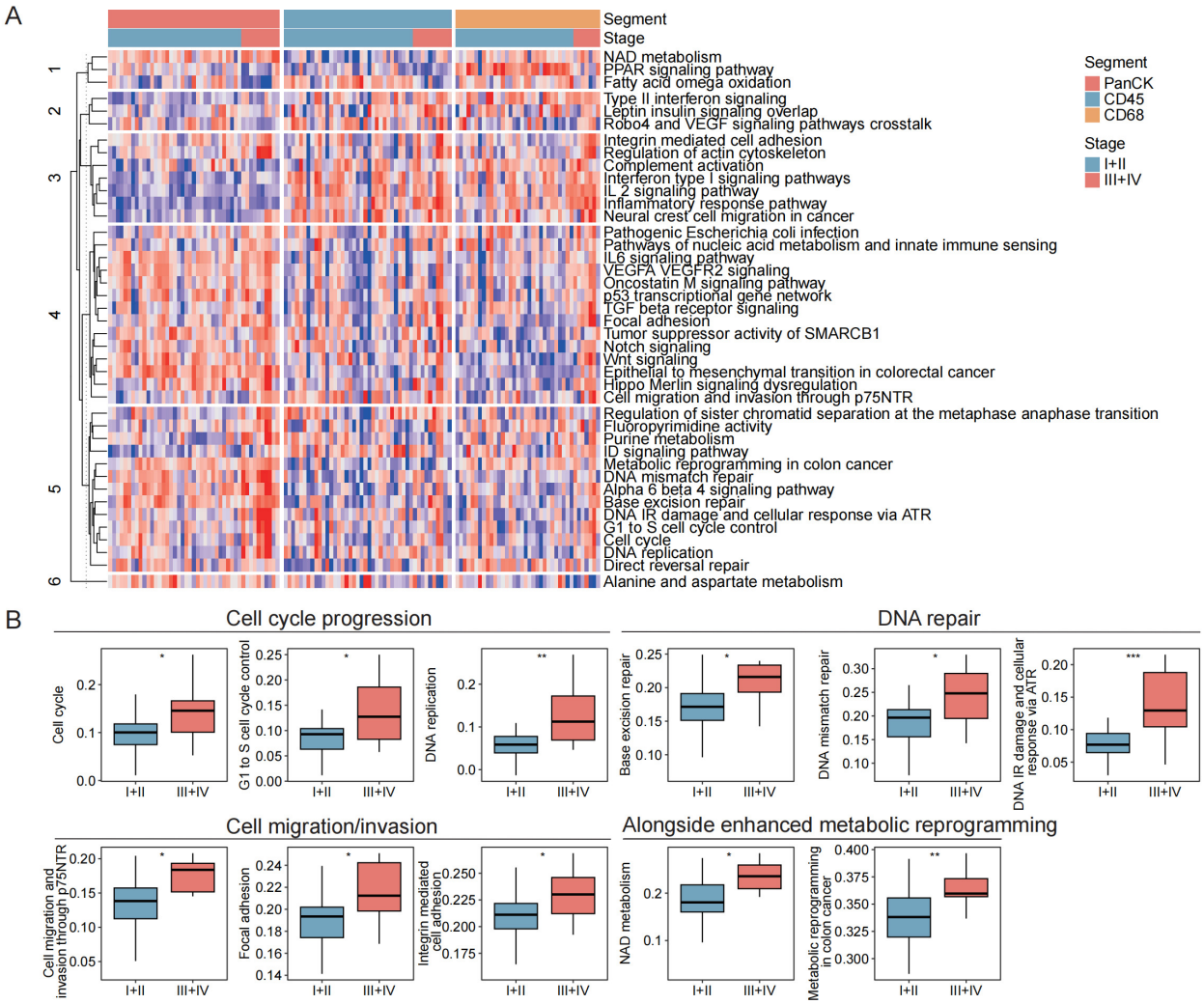

Fig. 4. Dysregulated signaling pathways associated with tumor stage in distinct tissue compartments. (A) Heatmap of unsupervised clustering based on ssGSEA scores derived from WikiPathways gene sets. Major clusters of dysregulated pathways are labeled with white horizontal lines. AOIs are grouped and ordered by tissue compartment and tumor stage. (B) Boxplots illustrating pathways that are significantly associated with stage within the PanCK^{+} tumor cell compartment. I+II stage (35 AOIs); III+IV stage (10 AOIs). ssGSEA, single sample gene set enrichment; AOIs, areas of illumination. *$p < 0.05$, **$p < 0.01$, ***$p < 0.001$.

Discussion

EGFR-mutated LUAD remains a major cause of cancer-related death, with marked clinical heterogeneity between early and late stages that directly affect treatment efficacy and prognosis [19,34,39]. Although EGFR-targeted therapies have greatly improved clinical management, acquired resistance and disease progression remain unresolved challenges [40,41]. This study combined bulk and spatial transcriptomics to characterize the molecular, spatial, and immune landscapes of early-stage (I+II) versus late-stage (III+IV) *EGFR*-mutated LUAD, revealing stage-specific molecular reprogramming, spatial compartmentalization of oncogenic signaling, and immune suppression mechanisms underlying disease progression.

Pathway and metabolic analyses confirmed that late-stage tumors displayed enhanced proliferative activity, marked by E2F, G2M, MYC signatures, along with upregulated MTORC1 signaling and an unfolded protein response, as well as a glycolytic metabolic shift consistent with the Warburg effect. Furthermore, based on the WikiPathways clustering results, the biological significance of the identified metabolic alterations was further elaborated. The pathway analysis revealed that late-stage tumors are characterized by activated programs related to proliferative, DNA repair, and metabolism, particularly highlighting enriched serine and purine metabolism, which clearly separates late-stage metabolic rewiring from early immune-dominant pathways. These stage-specific metabolic adaptations are functionally critical: enhanced serine and purine

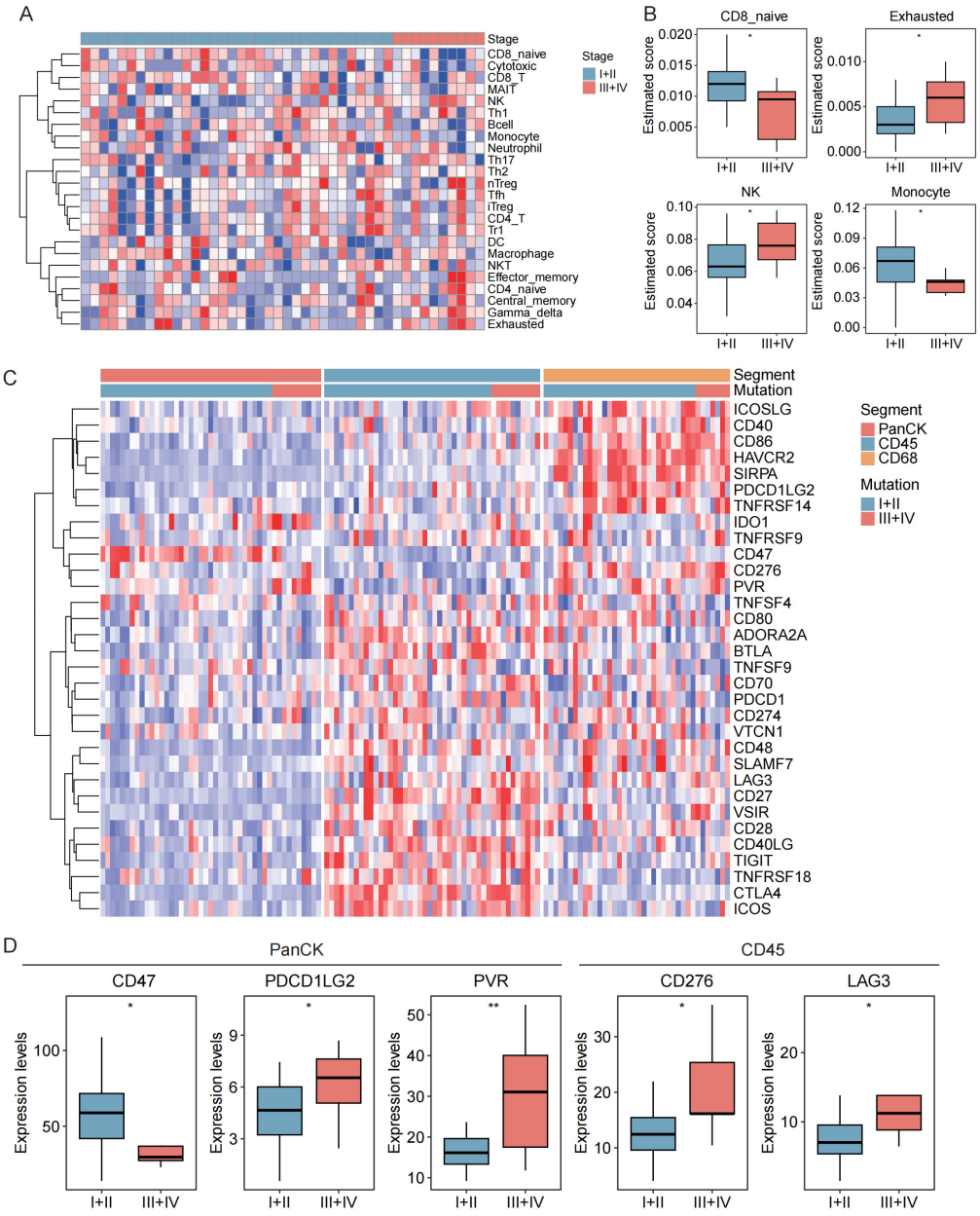

Fig. 5. Immune cell infiltration and immunomodulatory gene expression patterns across tumor stages in different compartments. (A) Heatmap of immune cell subpopulations inferred by the ImmuneCellAI algorithm, comparing early- and late-stage groups within the $CD45^+$ immune cell compartment. I+II stage (35 AOIs); III+IV stage (10 AOIs). (B) Boxplots showing immune cell types with significantly differential infiltration levels between the two stage groups in the $CD45^+$ immune cell compartment. (C) Heatmaps illustrating the expression of immunomodulatory genes across distinct compartments between early- and late-stage groups. The Wilcoxon rank-sum test (Mann-Whitney U test) was used for statistical comparisons. (D) Boxplots of log2-transformed and normalized expression levels of immunomodulatory genes in the $PanCK^+$ tumor cell and $CD45^+$ immune cell compartments, respectively, between the two stage groups. $*p < 0.05$, $**p < 0.01$.

metabolism provides essential nucleotide precursors and one-carbon units to sustain rapid tumor cell proliferation and genomic stability, enabling malignant cells to adapt to the harsh late-stage TME. Moreover, these metabolic dependencies are not merely passive byproducts of tumor progression but represent promising, targetable vulnerabilities [42,43]. Using DSP, three distinct tissue compartments were resolved: tumor cells ($PanCK^+$), immune cells ($CD45^+$), and macrophages ($CD68^+$). Late-stage tumor cells exhibited stronger activation of oncogenic pathways related to proliferation, MTORC1 signaling, hypoxia, angiogenesis, and EMT, consistent with bulk transcriptomic

results. Unsupervised pathway clustering demonstrated clear spatial and stage-specific modular activation: the tumor compartments drove progression-related signaling (VEGFA/VEGFR2, TGFβ, EMT, cell cycle, DNA repair), while immune and macrophage compartments dominated immunoregulatory and inflammatory programs. These findings suggest that tumor cell-autonomous molecular reprogramming is a key driver of late-stage progression.

Spatial immune profiling revealed a progressive immune suppression during disease progression. Late-stage tumors showed increased exhausted $CD8^+$ T cells, whereas early tumors contained more naïve $CD8^+$ T cells and monocytes. We also observed stage- and compartment-specific upregulation of immune checkpoints: *PDCD1LG2* (PD-L2) and *PVR* (*CD155*) were elevated in tumor cells, indicating that these cells actively secrete immunosuppressive signals to mediate immune evasion via multiple pathways. In contrast, *CD276* (B7-H3) and *LAG3* were increased in the immune compartment, suggesting that these molecules are induced by the TME and serve as markers of functionally exhausted immune cells. These molecules cooperatively inhibit phagocytosis and T cell function, thereby establishing an immunosuppressive TME. The binding of CD47 on tumor cells to SIRPα on macrophages inhibits macrophage-mediated phagocytosis [44,45,46]. PD-L2, a second ligand for PD-1, also inhibits T-cell activation [47,48,49]. PVR (CD155) emerges as a promising therapeutic target, especially in combination with anti-PD-1/PD-L1 blockade [50]. CD155 interacts with T cell immunoglobulin and ITIM domain (TIGIT), exerting immunosuppressive effects [51,52]. Additionally, B7-H3 can diminished the anti-tumor activity of T cells [53,54], while LAG3 is known to inhibit $CD8^+$ T cell function [55,56,57] and enhance the immunosuppressive behavior of regulatory T cells (Tregs) [58,59].

This study identified stage-specific molecular and immune signatures with potential prognostic and therapeutic implications. Metabolic and proliferative markers may help stratify high-risk patients, while the spatially compartmentalized oncogenic and immune pathways support combinatorial strategies targeting both tumor-intrinsic signaling (e.g., MTORC1, glycolysis) and immune checkpoints (e.g., PVR/TIGIT). Limitations include the relatively small size of the late-stage DSP sample, the focus on common *EGFR* mutations, and the observational nature of the study. Future investigations involving larger cohorts, additional mutation subtypes, and functional validation are needed to confirm causal mechanisms and therapeutic efficacy. DSP permitted the delineation of distinct compartments for tumor, immune, and macrophage compartments in *EGFR*-mutated LUAD across different stages. Although DSP technology limits direct analysis of inter-compartment interactions, the spatial expression data enable inference of potential tumor-immune and immune-stromal crosstalk. Specifically, upregulated exhausted $CD8^+$ T cell signatures and immune checkpoint molecules in late-stage tumors suggest a tumor-immune interplay related to immune escape. Follow-up studies using advanced single-cell spatial omics (e.g., CosMx Spatial Molecular Imaging) are planned to address the limitations of DSP and verify these interactions.

Conclusions

Integrated bulk and spatial transcriptomics reveal significant stage-dependent molecular, spatial, and immune alterations in *EGFR*-mutated LUAD. Early-stage tumors display active anti-tumor immunity, whereas late-stage tumors undergo extensive reprogramming toward proliferation, invasion, metabolic activation, and coordinated immune suppression characterized by T cell exhaustion and the upregulation of inhibitory checkpoints. These findings deepen the understanding of progression mechanisms and may provide candidate prognostic biomarkers and therapeutic targets for *EGFR*-mutated LUAD.

Availability of Data and Materials

DSP-derived datasets are deposited in the GSA-Human database with the accession number HRA011725 (https://ngdc.cncb.ac.cn/gsa-human/browse/HRA011725). Public RNA sequencing (RNA-seq) datasets were obtained from The Cancer Genome Atlas (TCGA) repository. All other datasets used or analyzed during the current study are available from the corresponding authors upon reasonable request.

Author Contributions

HLQ and ZXT conceived and designed the study and supervised the entire study. LYY and CC drafted the manuscript. LYY, CC, XRS, and SBL performed the data analysis. SBL and XRS collected the tumor samples. All authors have been involved in revising it critically for important intellectual content. All authors gave final approval of the version to be published. All authors have participated sufficiently in the work to take public responsibility for appropriate portions of the content and agreed to be accountable for all aspects of the work in ensuring that questions related to its accuracy or integrity.

Ethics Approval and Consent to Participate

All patients enrolled in this study provided written informed consent prior to participation. Ethical approval was granted by the Ethics Committee of the First Affiliated Hospital of Soochow University (approval number: [2025]480). All human-related procedures were performed in accordance with relevant guidelines and regulations of the First Affiliated Hospital of Soochow University and the Declaration of Helsinki.

Acknowledgment

Not applicable.

Funding

This study was supported by the Industry-Commissioned Project of Soochow University (No.P112205224) and Project of Jiangsu Province Engineering Research Center of Molecular Target Therapy and Companion Diagnostics in Oncology (No.SGK1202408).

Conflict of Interest

The authors declare no conflict of interest.

Supplementary Material

Supplementary material associated with this article can be found, in the online version, at https://doi.org/10.24976/Discov.Med.202638211.206.

References

[1] Herbst RS, Heymach JV, Lippman SM. Lung cancer. The New England Journal of Medicine. 2008; 359: 1367–1380. https://doi.org/10.1056/NEJMra0802714

[2] Cao W, Qin K, Liu B, Chen W. Cancer statistics in China: Epidemiology, risk factors, and prevention. Chinese Journal of Cancer Research = Chung-kuo Yen Cheng Yen Chiu. 2025; 37: 912–928. https://doi.org/10.21147/j.issn.1000-9604.2025.06.04

[3] Blechter B, Hsiung CA, Wang X, Zhang H, Seow WJ, Shi J, et al. Polygenic Risk Score and Lung Adenocarcinoma Risk Among Never-Smokers by EGFR Mutation Status: A Brief Report. Journal of Thoracic Oncology : Official Publication of the International Association for the Study of Lung Cancer. 2025; 20: 521–530. https://doi.org/10.1016/j.jtho.2024.11.019

[4] Shi Y, Au JSK, Thongprasert S, Srinivasan S, Tsai CM, Khoa MT, et al. A prospective, molecular epidemiology study of EGFR mutations in Asian patients with advanced non-small-cell lung cancer of adenocarcinoma histology (PIONEER). Journal of Thoracic Oncology : Official Publication of the International Association for the Study of Lung Cancer. 2014; 9: 154–162. https://doi.org/10.1097/JTO.0000000000000033

[5] Liu X, Ren Y, Fei Z, Shi Q, Lu L. Relationship between qualitative and quantitative parameters of three-dimensional computed tomography, EGFR gene mutation, and ALK gene rearrangement in GGO-associated lung adenocarcinoma and their prognostic value. Pathology Oncology Research : POR. 2025; 31: 1612081. https://doi.org/10.3389/pore.2025.1612081

[6] Maemondo M, Inoue A, Kobayashi K, Sugawara S, Oizumi S, Isobe H, et al. Gefitinib or chemotherapy for non-small-cell lung cancer with mutated EGFR. The New England Journal of Medicine. 2010; 362: 2380–2388. https://doi.org/10.1056/NEJMoa0909530

[7] Zhou C, Wu YL, Chen G, Feng J, Liu XQ, Wang C, et al. Erlotinib versus chemotherapy as first-line treatment for patients with advanced EGFR mutation-positive non-small-cell lung cancer (OPTIMAL, CTONG-0802): a multicentre, open-label, randomised, phase 3 study. The Lancet. Oncology. 2011; 12: 735–742. https://doi.org/10.1016/S1470-2045(11)70184-X

[8] Rosell R, Carcereny E, Gervais R, Vergnenegre A, Massuti B, Felip E, et al. Erlotinib versus standard chemotherapy as first-line treatment for European patients with advanced EGFR mutation-positive non-small-cell lung cancer (EURTAC): a multicentre, open-label, randomised phase 3 trial. The Lancet. Oncology. 2012; 13: 239–246. https://doi.org/10.1016/S1470-2045(11)70393-X

[9] Fu K, Xie F, Wang F, Fu L. Therapeutic strategies for EGFR-mutated non-small cell lung cancer patients with osimertinib resistance. Journal of Hematology & Oncology. 2022; 15: 173. https://doi.org/10.1186/s13045-022-01391-4

[10] Fang W, Wu L, Meng X, Yao Y, Zuo W, Yao W, et al. Sacituzumab Tirumotecan in EGFR-TKI-Resistant, *EGFR*-Mutated Advanced NSCLC. The New England Journal of Medicine. 2026; 394: 13–26. https://doi.org/10.1056/NEJMoa2512071

[11] Romaniello D, Morselli A, Marrocco I. Strategies to Overcome Resistance to Osimertinib in EGFR-Mutated Lung Cancer. International Journal of Molecular Sciences. 2025; 26: 2957. https://doi.org/10.3390/ijms26072957

[12] Zhou C, Jing Z, Liu W, Ma Z, Liu S, Fang Y. Prognosis of recurrence after complete resection in early-stage lung adenocarcinoma based on molecular alterations: a systematic review and meta-analysis. Scientific Reports. 2023; 13: 18710. https://doi.org/10.1038/s41598-023-42851-2

[13] Ahn JH, Choi SH, Park SH, Kim I, Park JH, Kim JY, et al. Longitudinal Analysis of Recurrence and Risk Factors of Early-Stage Resected Adenocarcinoma With Common EGFR Mutations: A Multicenter Retrospective Cohort Study in South Korea. Clinical Lung Cancer. 2025; 26: 314–323.e6. https://doi.org/10.1016/j.cllc.2025.02.016

[14] Chen T, Wen J, Li Y, Deng J, Zhong Y, Hou L, et al. Prognostic outcomes and recurrence patterns in resected stage I lung adenocarcinoma harbouring atypical epidermal growth factor receptor mutations. European Journal of Cardio-thoracic Surgery : Official Journal of the European Association for Cardio-thoracic Surgery. 2024; 65: ezad388. https://doi.org/10.1093/ejcts/ezad388

[15] Binnewies M, Roberts EW, Kersten K, Chan V, Fearon DF, Merad M, et al. Understanding the tumor immune microenvironment (TIME) for effective therapy. Nature Medicine. 2018; 24: 541–550. https://doi.org/10.1038/s41591-018-0014-x

[16] Morad G, Helmink BA, Sharma P, Wargo JA. Hallmarks of response, resistance, and toxicity to immune checkpoint blockade. Cell. 2021; 184: 5309–5337. https://doi.org/10.1016/j.cell.2021.09.020

[17] Hanahan D. Hallmarks of Cancer: New Dimensions. Cancer Discovery. 2022; 12: 31–46. https://doi.org/10.1158/2159-8290.CD-21-1059

[18] Quail DF, Joyce JA. Microenvironmental regulation of tumor progression and metastasis. Nature Medicine. 2013; 19: 1423–1437. https://doi.org/10.1038/nm.3394

[19] Gong Z, Du M, Li Y, Ye B, Huang Y, Gong H, et al. Machine learning identifies TIME subtypes linking EGFR mutations and immune states in lung adenocarcinoma. NPJ Digital Medicine. 2025; 8: 796. https://doi.org/10.1038/s41746-025-02172-2

[20] Madeddu C, Donisi C, Liscia N, Lai E, Scartozzi M, Macciò A. EGFR-Mutated Non-Small Cell Lung Cancer and Resistance to Immunotherapy: Role of the Tumor Microenvironment. International Journal of Molecular Sciences. 2022; 23: 6489. https://doi.org/10.3390/ijms23126489

[21] Hu LY, Zhuang WT, Chen MJ, Liao J, Wu DF, Zhang YX, et al. EGFR Oncogenic Mutations in NSCLC Impair Macrophage Phagocytosis and Mediate Innate Immune Evasion Through Up-Regulation of CD47. Journal of Thoracic Oncology : Official Publication of the International Association for the Study of Lung Cancer. 2024; 19: 1186–1200. https://doi.org/10.1016/j.jtho.2024.03.019

[22] Merritt CR, Ong GT, Church SE, Barker K, Danaher P, Geiss G,

et al. Multiplex digital spatial profiling of proteins and RNA in fixed tissue. Nature Biotechnology. 2020; 38: 586–599. https://doi.org/10.1038/s41587-020-0472-9

[23] Zhao Y, Wong L, Goh WWB. How to do quantile normalization correctly for gene expression data analyses. Scientific Reports. 2020; 10: 15534. https://doi.org/10.1038/s41598-020-72664-6

[24] Song X, Xiong A, Wu F, Li X, Wang J, Jiang T, et al. Spatial multi-omics revealed the impact of tumor ecosystem heterogeneity on immunotherapy efficacy in patients with advanced non-small cell lung cancer treated with bispecific antibody. Journal for Immunotherapy of Cancer. 2023; 11: e006234. https://doi.org/10.1136/jitc-2022-006234

[25] Hänzelmann S, Castelo R, Guinney J. GSVA: gene set variation analysis for microarray and RNA-seq data. BMC Bioinformatics. 2013; 14: 7. https://doi.org/10.1186/1471-2105-14-7

[26] Kanehisa M, Furumichi M, Sato Y, Matsuura Y, Ishiguro-Watanabe M. KEGG: biological systems database as a model of the real world. Nucleic Acids Research. 2025; 53: D672–D677. https://doi.org/10.1093/nar/gkae909

[27] Kanehisa M. Toward understanding the origin and evolution of cellular organisms. Protein Science : a Publication of the Protein Society. 2019; 28: 1947–1951. https://doi.org/10.1002/pro.3715

[28] Kanehisa M, Goto S. KEGG: kyoto encyclopedia of genes and genomes. Nucleic Acids Research. 2000; 28: 27–30. https://doi.org/10.1093/nar/28.1.27

[29] Miao YR, Zhang Q, Lei Q, Luo M, Xie GY, Wang H, et al. ImmuCellAI: A Unique Method for Comprehensive T-Cell Subsets Abundance Prediction and its Application in Cancer Immunotherapy. Advanced Science (Weinheim, Baden-Wurttemberg, Germany). 2020; 7: 1902880. https://doi.org/10.1002/advs.201902880

[30] Slenter DN, Kutmon M, Hanspers K, Riutta A, Windsor J, Nunes N, et al. WikiPathways: a multifaceted pathway database bridging metabolomics to other omics research. Nucleic Acids Research. 2018; 46: D661–D667. https://doi.org/10.1093/nar/gkx1064

[31] Roelands J, van der Ploeg M, Ijsselsteijn ME, Dang H, Boonstra JJ, Hardwick JCH, et al. Transcriptomic and immunophenotypic profiling reveals molecular and immunological hallmarks of colorectal cancer tumourigenesis. Gut. 2023; 72: 1326–1339. https://doi.org/10.1136/gutjnl-2022-327608

[32] Li R, Li N, Yang Q, Tong X, Wang W, Li C, et al. Spatial transcriptome profiling identifies DTX3L and BST2 as key biomarkers in esophageal squamous cell carcinoma tumorigenesis. Genome Medicine. 2024; 16: 148. https://doi.org/10.1186/s13073-024-01422-4

[33] Charoentong P, Finotello F, Angelova M, Mayer C, Efremova M, Rieder D, et al. Pan-cancer Immunogenomic Analyses Reveal Genotype-Immunophenotype Relationships and Predictors of Response to Checkpoint Blockade. Cell Reports. 2017; 18: 248–262. https://doi.org/10.1016/j.celrep.2016.12.019

[34] Fu F, Shang J, Yan Y, Jiang H, Han H, Yuan H, et al. Genomic and transcriptomic dynamics in the stepwise progression of lung adenocarcinoma. Cell Research. 2025; 35: 1037–1055. https://doi.org/10.1038/s41422-025-01200-w

[35] Yu C, Shi C, Zhou H, Li N, Ma R, Liu S, et al. Spatially resolved whole-transcriptomic profiling of EGFR-mutated lung adenocarcinomas stratified by PD-L1 expression. Cellular Oncology (Dordrecht, Netherlands). 2025; 49: 2. https://doi.org/10.1007/s13402-025-01143-9

[36] Pickup MW, Mouw JK, Weaver VM. The extracellular matrix modulates the hallmarks of cancer. EMBO Reports. 2014; 15: 1243–1253. https://doi.org/10.15252/embr.201439246

[37] Di Chiaro P, Nacci L, Arco F, Brandini S, Polletti S, Palamidessi A, et al. Mapping functional to morphological variation reveals the basis of regional extracellular matrix subversion and nerve invasion in pancreatic cancer. Cancer Cell. 2024; 42: 662–681.e10. https://doi.org/10.1016/j.ccell.2024.02.017

[38] Curvello R, Hauser S, Seifert M, Barlow CK, Steele JR, Salisbury E, et al. GOT1 Inhibition Induces Extracellular Matrix Remodeling in Pancreatic Cancer. Advanced Science (Weinheim, Baden-Wurttemberg, Germany). 2026; 13: e16578. https://doi.org/10.1002/advs.202516578

[39] Borgeaud M, Olivier T, Bar J, Saw SPL, Parikh K, Banna GL, et al. Personalized care for patients with EGFR-mutant nonsmall cell lung cancer: Navigating early to advanced disease management. CA: a Cancer Journal for Clinicians. 2025; 75: 387–409. https://doi.org/10.3322/caac.70024

[40] Zhou X, Zeng L, Huang Z, Ruan Z, Yan H, Zou C, et al. Strategies Beyond 3rd EGFR-TKI Acquired Resistance: Opportunities and Challenges. Cancer Medicine. 2025; 14: e70921. https://doi.org/10.1002/cam4.70921

[41] Meador CB, Hata AN. Acquired resistance to targeted therapies in NSCLC: Updates and evolving insights. Pharmacology & Therapeutics. 2020; 210: 107522. https://doi.org/10.1016/j.pharmthera.2020.107522

[42] Geng P, Ye F, Dou P, Hu C, He J, Zhao J, et al. HIF-1α-HPRT1 axis promotes tumorigenesis and gefitinib resistance by enhancing purine metabolism in EGFR-mutant lung adenocarcinoma. Journal of Experimental & Clinical Cancer Research : CR. 2024; 43: 269. https://doi.org/10.1186/s13046-024-03184-8

[43] Shunxi W, Xiaoxue Y, Guanbin S, Li Y, Junyu J, Wanqian L. Serine Metabolic Reprogramming in Tumorigenesis, Tumor Immunity, and Clinical Treatment. Advances in Nutrition (Bethesda, Md.). 2023; 14: 1050–1066. https://doi.org/10.1016/j.advnut.2023.05.007

[44] Logtenberg MEW, Scheeren FA, Schumacher TN. The CD47-SIRPα Immune Checkpoint. Immunity. 2020; 52: 742–752. https://doi.org/10.1016/j.immuni.2020.04.011

[45] Yousefi-Hashemabad MJ, Kamroo A, Rezvanimehr A, Saleki K, Barootchi E, Mehrani A, et al. CD47/SIRPα Immune Checkpoint Modulation: A Synergistic Strategy for Next-Generation CAR Therapies. Molecular Cancer Therapeutics. 2026; 25: 912–923. https://doi.org/10.1158/1535-7163.MCT-25-0531

[46] Reischer A, Leutbecher A, Hiller B, Perini E, White K, Hernández-Cáceres A, et al. Targeted CD47 checkpoint blockade using a mesothelin-directed antibody construct for enhanced solid tumor-specific immunotherapy. Cancer Immunology, Immunotherapy : CII. 2025; 74: 214. https://doi.org/10.1007/s00262-025-04032-0

[47] Latchman Y, Wood CR, Chernova T, Chaudhary D, Borde M, Chernova I, et al. PD-L2 is a second ligand for PD-1 and inhibits T cell activation. Nature Immunology. 2001; 2: 261–268. https://doi.org/10.1038/85330

[48] Patwari A, Nishizaki D, Jensen T, DePietro P, Pabla S, Kato S, et al. PD-L2 Landscape and Correlation with Outcome: An Immunomic Analysis. JCO Oncology Advances. 2026; 3: e2500151. https://doi.org/10.1200/oa-25-00151

[49] Ontiveros CO, Garcia MG, Murray CE, Deng Y, Bai H, Tanner C, et al. Anti-PD-L2 immunotherapy is efficacious against melanoma in aged hosts through IL-17 and IFNγ signalling. Nature Communications. 2025; 16: 10176. https://doi.org/10.1038/s41467-025-65025-2

[50] Liu X, Sun Y, Lin B, Xiong H, Lu X, Tan B, et al. Pan-cancer analysis identifies CD155 as a promising target for CAR-T cell therapy. Genome Medicine. 2025; 17: 64. https://doi.org/10.1186/s13073-025-01490-0

[51] Stanietsky N, Simic H, Arapovic J, Toporik A, Levy O, Novik A, et al. The interaction of TIGIT with PVR and PVRL2 inhibits human NK cell cytotoxicity. Proceedings of the National Academy of Sciences of the United States of America. 2009; 106: 17858–17863. https://doi.org/10.1073/pnas.0903474106

[52] Yu X, Harden K, Gonzalez LC, Francesco M, Chiang E, Irving B, et al. The surface protein TIGIT suppresses T cell activation by promoting the generation of mature immunoregulatory dendritic cells. Nature Immunology. 2009; 10: 48–57. https://doi.org/10.1038/ni.1674

[53] Lee YH, Martin-Orozco N, Zheng P, Li J, Zhang P, Tan H, et al. Inhibition of the B7-H3 immune checkpoint limits tumor growth by enhancing cytotoxic lymphocyte function. Cell Research. 2017; 27: 1034–1045. https://doi.org/10.1038/cr.2017.90

[54] Picarda E, Ohaegbulam KC, Zang X. Molecular Pathways: Targeting B7-H3 (CD276) for Human Cancer Immunotherapy. Clinical Cancer Research : an Official Journal of the American Association for Cancer Research. 2016; 22: 3425–3431. https://doi.org/10.1158/1078-0432.CCR-15-2428

[55] Matsuzaki J, Gnjatic S, Mhawech-Fauceglia P, Beck A, Miller A, Tsuji T, et al. Tumor-infiltrating NY-ESO-1-specific CD8+ T cells are negatively regulated by LAG-3 and PD-1 in human ovarian cancer. Proceedings of the National Academy of Sciences of the United States of America. 2010; 107: 7875–7880. https://doi.org/10.1073/pnas.1003345107

[56] Andrews LP, Butler SC, Cui J, Cillo AR, Cardello C, Liu C, et al. LAG-3 and PD-1 synergize on $CD8^+$ T cells to drive T cell exhaustion and hinder autocrine IFN-γ-dependent antitumor immunity. Cell. 2024; 187: 4355–4372.e22. https://doi.org/10.1016/j.cell.2024.07.016

[57] Cillo AR, Cardello C, Shan F, Karapetyan L, Kunning S, Sander C, et al. Blockade of LAG-3 and PD-1 leads to co-expression of cytotoxic and exhaustion gene modules in $CD8^+$ T cells to promote antitumor immunity. Cell. 2024; 187: 4373–4388.e15. https://doi.org/10.1016/j.cell.2024.06.036

[58] Yano H, Andrews LP, Workman CJ, Vignali DAA. Intratumoral regulatory T cells: markers, subsets and their impact on antitumor immunity. Immunology. 2019; 157: 232–247. https://doi.org/10.1111/imm.13067

[59] Kim D, Kim G, Yu R, Lee J, Kim S, Gleason MR, et al. Inhibitory co-receptor Lag3 supports $Foxp3^+$ regulatory T cell function by restraining Myc-dependent metabolic programming. Immunity. 2024; 57: 2634–2650.e5. https://doi.org/10.1016/j.immuni.2024.08.008